Separation Science and Technology
Publication details, including instructions for authors and subscription information:
http://www.informaworld.com/smpp/title~content=t713708471

Simulation of Unstirred Batch Ultrafiltration System Based on Analytical Solution of Boundary Layer Equation

Aniruddha Poddar[a]; Chiranjib Bhattacharjee[a]; Siddhartha Datta[a]
[a] DEPARTMENT OF CHEMICAL ENGINEERING, JADAVPUR UNIVERSITY, CALCUTTA, INDIA

Online publication date: 15 September 1999

To cite this Article Poddar, Aniruddha , Bhattacharjee, Chiranjib and Datta, Siddhartha(1999) 'Simulation of Unstirred Batch Ultrafiltration System Based on Analytical Solution of Boundary Layer Equation', Separation Science and Technology, 34: 13, 2485 — 2500
To link to this Article: DOI: 10.1081/SS-100100786
URL: http://dx.doi.org/10.1081/SS-100100786

SEPARATION SCIENCE AND TECHNOLOGY, **34**(13), pp. 2485–2500, 1999

Simulation of Unstirred Batch Ultrafiltration System Based on Analytical Solution of Boundary Layer Equation

ANIRUDDHA PODDAR, CHIRANJIB BHATTACHARJEE, and SIDDHARTHA DATTA*

DEPARTMENT OF CHEMICAL ENGINEERING
JADAVPUR UNIVERSITY
CALCUTTA-700 032, INDIA

ABSTRACT

A mass transfer model based on an unsteady-state mass balance over the concentration boundary layer, coupled with diffusive backtransport opposing the ultrafiltrate flux, has been developed in the present study. This model can be used to simulate flux and rejection at any desired time in an unstirred batch ultrafiltration module. This model uses the semi-infinite consideration to solve the governing partial differential equation by the Laplace transform technique, which gives the analytical solution of the concentration profile. In the partial differential equation, volumetric flux is assumed to be constant in accordance with pseudosteady-state assumption, often used in diffusive mass transfer analysis. Once the analytical expression for the concentration profile has been found, an iterative technique has been used in conjunction with other membrane and solute properties to predict the flux and rejection at any desired time under a specified operating condition. Concentration profiles as a function of time for different experiments are also computed in order to analyze the effect of different operating parameters on the concentration boundary layer. The prediction from this model is found to be in good agreement with the experimental results obtained during ultrafiltration of PEG-6000 in an unstirred batch module using a cellulose acetate membrane of MWCO-5000, and in most cases the variation of concentration within the boundary layer is found to be limited within a very short distance over the membrane surface.

* To whom correspondence should be addressed.

INTRODUCTION

Over the past few decades, ultrafiltration (UF), a pressure-driven membrane process, has emerged as a viable process for the concentration or separation of moderate to high molecular weight solutes from solution. In ultrafiltration, the dispersed phase (i.e., solute) passes less readily through the membrane than the solvent. The reasons for this may be classified as follows:

1. The solute may be adsorbed on the surface of the filter and its pore (primary adsorption).
2. The solute may be retained within the pores (blocking).
3. The solute may be mechanically retained (sieving).

One of the problems found in ultrafiltration is the marked decline of permeate flux with time. This is mostly attributed to the phenomenon of concentration polarization, the accumulation of the retained solute on the high-pressure side of the membrane surface. This layer of retained solute is an additional resistance to solvent flow so that the solvent flux is reduced at any pressure from the ideal level.

Trettin and Doshi (1) developed a theory essentially based on gel layer formation and proposed an integral model which was an effort for unification of macromolecular ultrafiltration theories with classical filtration theory. This model differs substantially from the Shen and Probstein (2) model. Experiments with unstirred batch cell using BSA solution were performed to verify this model (3). A summary of governing transport and adsorption phenomena in porous membrane ducts under isothermal condition is given in the review article by Belfort and Nagata (4). Theories based on hypothetical boundary layer (film) or polarized gel layer mainly govern the studies to date. However, some recent theories like those based on the leaky membrane concept and solute–solute or solute–membrane interaction have gained importance. The effect of concentration polarization is very detrimental from the industrial point of view. This is summarized by Aimar and Sanchez (5). In many membrane separation processes the diffusional phenomenon plays an important role in the transport mechanism of solutes. Various mechanisms have been distinguished to describe the transport in the membranes, transport through bulk material (dense membrane), Knudsen diffusion in narrow pores, viscous flow in wide pores, or surface diffusion along pore walls. Models have been derived for all these and are given in a review article (6).

A computer simulation to calculate membrane performance data for a rectangular slit configuration was discussed by Leburn et al. (7). This was

achieved by coupling the surface force-pore flow model for membrane transport and the concentration polarization model through a boundary condition. The resulting differential equations from both the models were solved by a finite difference technique. Recently, very good work in formulating the concentration polarization phenomenon was reported by Song and Elimelech (8). Their model applies to the concentration polarization of noninteracting particles in a crossflow filtration system. The theory reveals that the extent of concentration polarization is characterized by a dimensionless number, called the filtration number. There is a critical value of this number for a given suspension and operating condition, below which a polarization layer exists directly over the membrane surface. The wall particle concentration is determined by pressure and temperature. At a higher filtration number a cake layer of retained particles forms between the polarized layer and the membrane surface. Mathematical models have been constructed for both cases, and an analytical solution for permeate flux was derived. The effects of natural convection instability on membrane performance in dead-end and crossflow ultrafiltration were recently discussed in an interesting manner by Youm et al. (9). A mass transfer correlation for the mixed convection membrane system was also presented. Various works regarding the analysis of mass transfer in the boundary layer for batch, continuous, and crossflow ultrafiltration and prediction of flux and rejection have been reported in the literature (10–13). A significant work regarding modeling of concentration polarization and depolarization with high frequency backpulsing was reported by Redkar et al. (14). Recently a unified model for prediction of flux in stirred and unstirred batch ultrafiltration was also reported (15).

Most of the work reported in the literature is based on some sort of numerical solution of the boundary layer mass transfer process and its associated phenomena like gel formation, osmotic pressure development, etc. So far very little work has been reported in the literature about the analytical solution of boundary layer partial differential equation, and most of them involve certain limitations/assumptions. The present work was undertaken in an attempt to simulate flux and rejection behavior during ultrafiltration of PEG-6000 in an unstirred batch cell using an asymmetric cellulose acetate membrane of 5000 MWCO. The main feature of the present work is that an analytical solution of a governing boundary layer partial differential equation with the pseudosteady-state assumption has been derived. The concentration profile as obtained from the model equation has been coupled with an osmotic pressure model and irreversible thermodynamics to predict flux and rejection at any instant under specified operating conditions. The predicted results are found to be in good agreement with the experimental data, and the observed average deviation in all cases is found to be within $\pm 10\%$.

THEORY

Estimation of Membrane Surface Concentration and Characterization of Membrane

The membrane surface concentration has been estimated by using the osmotic pressure model:

$$J = \frac{\Delta P - \sigma\,\Delta\pi}{\mu R_m} \tag{1}$$

where $\Delta\pi = \pi(c_m) - \pi(c_p)$.

The membrane hydraulic resistance is estimated through a series of water runs after allowing for initial compaction. The osmotic pressure of a macromolecular solution as a function of concentration is determined by using Flory's equation (16):

$$\pi = \frac{RT}{V_1}\left[\ln\gamma_1 + \left(1 - \frac{1}{x}\right)\gamma_2 + x_1\gamma_2^2\right] \tag{2}$$

where $x = V_p M_p / V_1 M_1$, $\gamma_2 = c/\rho_p$, and $\gamma_1 = 1 - \gamma_2$. For PEG, $\rho_p = 1125$ kg/m^3. The value of parameter x_1 depends on the type of polymer–solvent interaction ($x_1 = 0.45$ for PEG) (17).

The viscosity of PEG-6000 in water solution at 25°C can be related to a polynomial function of concentration in the form (10):

$$\mu = (0.85 + 0.01446c + 2.734 \times 10^{-4}\,c^2 - 4.276 \times 10^{-6}\,c^3 + 2.84 \times 10^{-6}\,c^4)/1000.0 \tag{3}$$

Direct solution of Eq. (1) for c_m coupled with Eq. (2) was not possible because the reflection coefficient (σ) still has not been determined. The "real" rejection can be obtained from nonequilibrium thermodynamics (18) with the help of the following equation:

$$R_r = 1 - \frac{c_p}{c_m} = \frac{\sigma(1 - F)}{1 - \sigma F} \tag{4}$$

where $F = \exp\{-(1 - \sigma)J/P_m\}$.

The membrane parameters, viz., reflection coefficient and solute permeability, have been determined by modification of the scheme outlined by Nakao and Kimura (18). The iterative technique that has been followed is given below:

(i) Assuming a σ value, Eq. (1) together with Eq. (2) is solved to determine the membrane surface concentration.

(ii) P_m is calculated from Eq. (4) for the above-mentioned assumed value of σ, using experimental values of J and c_p. This procedure is followed to calculate P_m values for all the experiments.

MARCEL DEKKER, INC.
270 Madison Avenue, New York, New York 10016

(iii) Standard deviation in the P_m values is now calculated, again for the same assumed value of σ.

(iv) In this way, different σ values are assumed and the procedure is repeated to calculate the standard deviation for all of them. The Fibonacci search technique is used to locate the σ value after minimization of standard deviation.

(v) Average of all P_m values for different experiments gives the correct solute permeability.

(vi) Using the above σ value, determined in Step (iv), Step (i) is repeated and the c_m value obtained is checked with the previous one. If the difference is more than the allowable tolerance, Step (i) to Step (v) is again repeated with the new c_m value as obtained from Step (i). This procedure is continued until convergence in c_m is obtained.

Development of the Model Equation

The present study deals with the analytical solution of the parabolic partial differential equation governing boundary layer mass transfer in the case of an unstirred batch ultrafiltration module. The pseudosteady-state assumption, as often used in many diffusive mass transfer problem, is first used to get the concentration profile. Then this analytical expression, coupled with irreversible thermodynamics and the osmotic pressure model, is used to simulate flux and rejection at any time under specified operating conditions.

Unsteady-state mass balance over the concentration boundary layer gives rise to the following equation:

$$\frac{\partial c}{\partial t} = J\frac{\partial c}{\partial z} + D\frac{\partial^2 c}{\partial z^2} \tag{5}$$

The above equation assumes constant diffusivity and density, and it is solved by considering the *semi-infinite* model under the following initial and boundary conditions:

$$\begin{aligned} &\text{At } t = 0,\ c = c_b \text{ for all } z;\ c(z, 0) = c_b,\ z \geq 0 \\ &\text{At } z = 0,\ c = c_m \text{ for all } t;\ c(0, t) = c_m,\ t > 0 \\ &\text{As } z \to \infty,\ c = c_b \text{ for all } t;\ c(\infty, t) = c_b,\ t \geq 0 \end{aligned} \tag{6}$$

The "pseudosteady-state" assumption is considered, according to which the volumetric flux and the membrane surface concentration can be assumed to be constant. Using the Laplace transformation technique Eq. (5) reduces to

$$D\frac{d^2\bar{c}}{dz^2} + J\frac{d\bar{c}}{dz} = s\bar{c} - c(z, 0) \tag{7}$$

MARCEL DEKKER, INC.
270 Madison Avenue, New York, New York 10016

By using the initial condition in Eq. (7), it reduces to

$$D\frac{d^2\bar{c}}{dz^2} + J\frac{d\bar{c}}{dz} - s\bar{c} = -c_b \tag{8}$$

Equation (8) is an ordinary differential equation with z as an independent variable and $\bar{c}$ as a dependent variable. The solution of the above equation is

$$\bar{c} = A' \exp(\alpha z) + B' \exp(\beta z) + \frac{c_b}{s} \tag{9}$$

where A' and B' are constants which are to be evaluated by the boundary conditions (6), and

$$\alpha = \frac{-J - \sqrt{J^2 + 4Ds}}{2D}$$

is negative for all values of J and D, whereas

$$\beta = \frac{-J + \sqrt{J^2 + 4Ds}}{2D}$$

is positive for all values of J and D.

By using the boundary conditions (6) in Eq. (9), it is found that A' reduces to zero and takes the following form:

$$\bar{c} = B' \exp(\beta z) + \frac{c_b}{s} \tag{10}$$

By substituting boundary condition (6) in Eq. (10), it is found that $B' = (c_m - c_b)/s$, and hence Eq. (10), reduces to

$$\bar{c} = \frac{c_m - c_b}{s} \exp\left(-\frac{Jz}{2D} - \frac{\sqrt{J^2 + 4Ds}}{2D} z\right) + \frac{c_b}{s} \tag{11}$$

By taking the inverse Laplace transform of Eq. (11) and replacing $Jz/2D$ by B, it can be written as

$$c = c_b + (c_m - c_b) \exp(-B) L^{-1}[f(s)] \tag{12}$$

where

$$f(s) = \frac{1}{s} \exp\left(-\frac{\sqrt{J^2 + 4Ds}}{2D} z\right) \tag{13}$$

By taking the inverse Laplace transform of Eq. (13), it can be reduced to the following form after using the property of the shifting theorem:

$$f(t) = \exp\left(-\frac{J^2}{4D} t\right) L^{-1}[F(s)] \tag{14}$$

MARCEL DEKKER, INC.
270 Madison Avenue, New York, New York 10016

where

$$F(s) = \frac{1}{\left(s - \frac{J^2}{4D}\right)} \exp\left(-\frac{z}{\sqrt{D}}\sqrt{s}\right) \tag{15}$$

Factorizing $[s - (J^2/4D)]$ into $[\sqrt{s} + (J/2\sqrt{D})]$ $[\sqrt{s} - (J/2\sqrt{D})]$ and reducing $F(s)$ into partial fractions and then taking the inverse Laplace transform of Eq. (15) and rearranging the solution by using the property of the error function, the equation takes the form

$$F(t) = \exp\left(\frac{J^2}{4D}t\right)\left[\cosh(B) - \frac{1}{2}\left\{\begin{array}{l}\exp(B)\,\mathrm{erf}\left(\frac{J}{2}\sqrt{\frac{t}{D}} + \frac{z}{2\sqrt{Dt}}\right) + \\ \exp(-B)\,\mathrm{erf}\left(-\frac{J}{2}\sqrt{\frac{t}{D}} + \frac{z}{2\sqrt{Dt}}\right)\end{array}\right\}\right] \tag{16}$$

Putting $F(t)$ in Eq. (14) and then $f(t)$ in Eq. (12) with the substitution of $(J/2)\sqrt{t/D}$ as Q and $z/2\sqrt{Dt}$ as S, the final solution can be written as

$$c = c_b + (c_m - c_b)\exp(-B)\left[\cosh(B) - \frac{1}{2}\left\{\begin{array}{l}\exp(B)\,\mathrm{erf}(S + Q) + \\ \exp(-B)\,\mathrm{erf}(S - Q)\end{array}\right\}\right] \tag{17}$$

Simulation of Flux and Rejection

Once the expression for the concentration profile under the pseudosteady-state assumption has been found, it can be used in conjunction with Eqs. (1) and (4) to predict flux and rejection at any instant under specified operating conditions. The following iteration scheme has been suggested:

(i) At $t = 0$, $c_p^{(0)} = c_b$, and $c_m^{(0)} = c_b$, $J^{(0)}$ is found from Eq. (1).

(ii) At $t = t + \Delta t$, the concentration profile is evaluated based on previous values of $J^{(0)}$, $c_m^{(0)}$, and $c_p^{(0)}$ from Eq. (17). The derivative $\partial c/\partial z$ at $z = 0$ and at the present time t can be found either numerically, using the finite difference formula, or analytically by substituting the infinite series expression for the error function in Eq. (17).

(iii) The present value of the volumetric flux is found from

$$J^{(n)} = -\frac{D}{c_m^{(0)} - c_b^{(0)}}\left(\frac{\partial c}{\partial z}\right)_{z=0} \tag{18}$$

(iv) The ratio $c_p^{(n)}/c_m^{(n)}$ is found from Eq. (4).

(v) $c_p^{(n)}$ and $c_m^{(n)}$ are solved from Eq. (1) by using the values of $c_p^{(n)}/c_m^{(n)}$.

(vi) Assigning $J^{(n)}$, $c_p^{(n)}$, and $c_m^{(n)}$ to $J^{(0)}$, $c_p^{(0)}$, and $c_m^{(0)}$, respectively, all steps from (ii) are repeated up to any desired time.

EXPERIMENTAL

Unstirred batch cell data generated in this study has been used to test the validity of the developed model. For the purpose of experimentation, an asymmetric cellulose acetate membrane of 5000 MWCO with a stainless steel support having fine pores has been used. The membrane was imported for the present study directly from Millipore Corporation, Bedford, MA 01730, USA. The product code of the membrane is Millipore: PLCC 09005. The membrane used for this study was a flat disk, asymmetric, anisotropic, and hydrophilic in nature. The diameter of the membrane used in the test cell was 43 mm, and the effective filtration area was 8.24×10^{-4} m^2. The original diameter of the membrane was 90 mm, from which a circular piece of the desired diameter was cut. The membrane was manufactured from low binding regenerated cellulose acetate. The membrane is capable of withstanding a pH range of 2 to 10 with a maximum allowable temperature of 95°C.

Polyethylene glycol-6000 was used as the solute in this study. It was obtained from Sisco Research Laboratories Pvt. Ltd., Bombay, India. The average molecular weight was 6000 with a polydispersity in the 5000 to 7000 molecular weight range. The concentration levels of the PEG solution used were 30, 45, and 60 kg/m^3 with pressure levels of 588.6, 490.5, and 392.4 kPa. The total permeate collection was measured as a function of time with a high precision measuring cylinder. The concentration of PEG was measured by the viscosity index calibration method, for which an optical refractomer with accuracies of ± 0.001 by reading and ± 0.0001 by eye estimation were used in the experiments.

The test cell used in this study was fabricated in our workshop without any stirring facility. The material used for construction was Grade SS316 stainless steel. The capacity of the test cell was 85 mL, and it was pressurized by a N_2 gas cylinder through a pressure regulator. The maximum testing pressure was 1000 kPa. The whole experimental setup was immersed in a constant temperature bath at 25°C.

RESULTS AND DISCUSSION

Some care must be taken during the simulation of flux and rejection according to the iteration scheme described here. Some time lag is inherent in the iteration scheme, as suggested above, so it is necessary to take Δt sufficiently small in the iteration process. The predicted values of J and c_p are found to be well in agreement with the experimental data for $\Delta t = 0.1$ second. This has

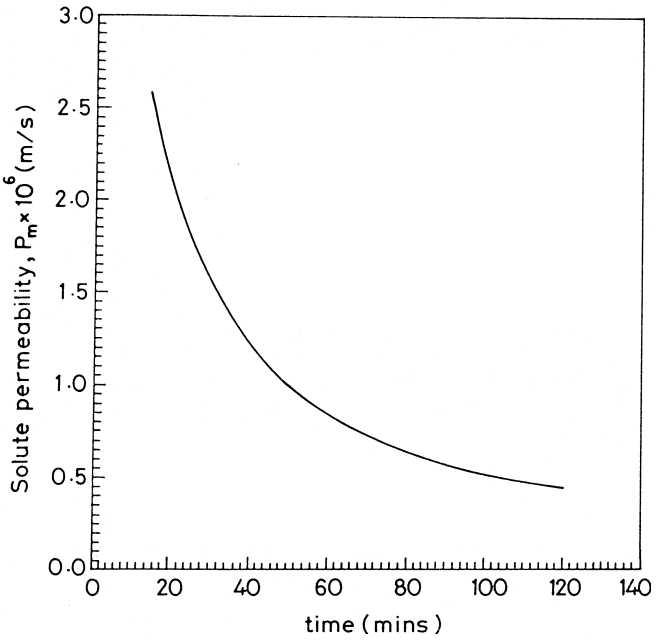

FIG. 1 Variation of solute permeability with time (results obtained at 25°C, with $R_m = 1.00014 \times 10^{14}$ m^{-1}. Reflection coefficient = 0.9615).

been found to be true for all experimental runs up to $\Delta t = 5$ seconds. Some erratic values may result after that, particularly for high flux data obtained at higher pressures. For the experimental run at $\Delta P = 490.5$ kPa, a stable solution was found even up to $\Delta t = 10$ seconds. But for $\Delta P = 588.6$ kPa, the solution tends to blow up if Δt is more than 5 seconds.

As mentioned earlier, membrane characterization by minimization of the standard deviation by the Fibonacci search technique was found to give a reflection coefficient of 0.9615. The solute permeability was obtained as a function of time, and its variation with time is shown in Fig. 1. The solute permeability decreases with time mainly because of osmotic pressure buildup. A decrease in solute permeability may also take place due to the hindrance effect occurring adjacent to the membrane surface owing to the increased concentration of solute molecules as a function of time—a phenomena associated with concentration polarization. The reflection coefficient, which is a property of the membrane, was found to be invariant with time.

Figure 2 shows the concentration profile as a function of time for a particular run under a specified set of operating conditions. Initially, a flat concentration profile exists throughout the region. After the ultrafiltration process is started, the profile develops very quickly. The concentration near the membrane increases more rapidly compared to the region further away from the membrane. The figure also shows that the concentration at any point within

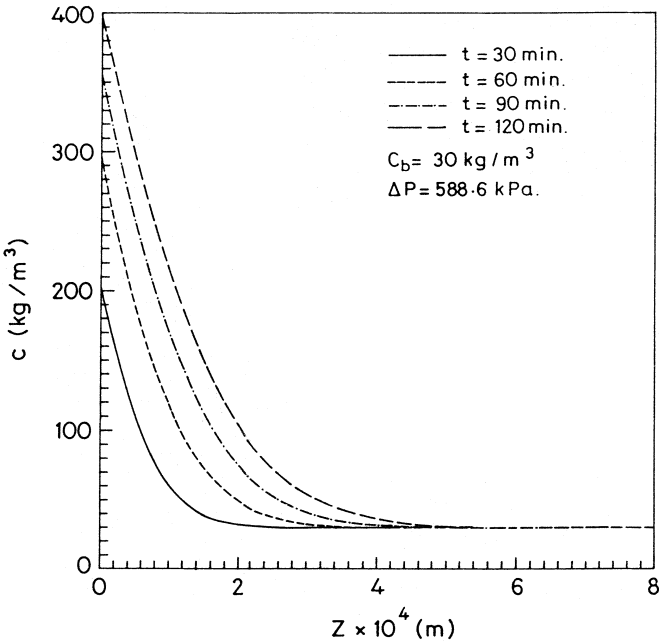

FIG. 2 Development of concentration profile with time (results obtained at 25°C, with $c_b = 30$ kg/m^3 and $\Delta P = 588.6$ kPa. Solute diffusivity $= 1.50788 \times 10^{-10}$ m^2/s, $R_m = 1.00014 \times 10^{14}$ m^{-1}, and $\sigma = 0.9615$).

the boundary layer increases with time. This is in accordance with the concentration polarization phenomenon because as time increases, the sieving action of the membrane increases, and this results in an increase of solute concentration at all points in the boundary layer. Moreover, the figure also suggests that the "apparent" boundary layer thickness also increases with time. Although the boundary layer is assumed to exist over infinite length, the figure shows that an appreciable change in concentration occurs within a short distance from the membrane surface, indicating that the concentration gradient is very high near the membrane and slowly becomes flat after an "apparent" thickness of the order of 1 mm.

The variation of membrane surface concentration with time at different operating pressures with the bulk concentration remaining constant as shown in Fig. 3. The membrane surface concentration initially increases very rapidly, but its rate of increase diminishes with time and after a short span of time almost becomes flat. This is due to the fact that as time increases the membrane surface concentration shows a positive trend, resulting in an increase in the osmotic pressure differential which opposes the applied pressure differential. This results in a decrease of the effective driving force, which gives rise to a retarded volumetric flux and hence to a lower solute transportation rate to the membrane surface. In addition to the above effect, concentration polarization

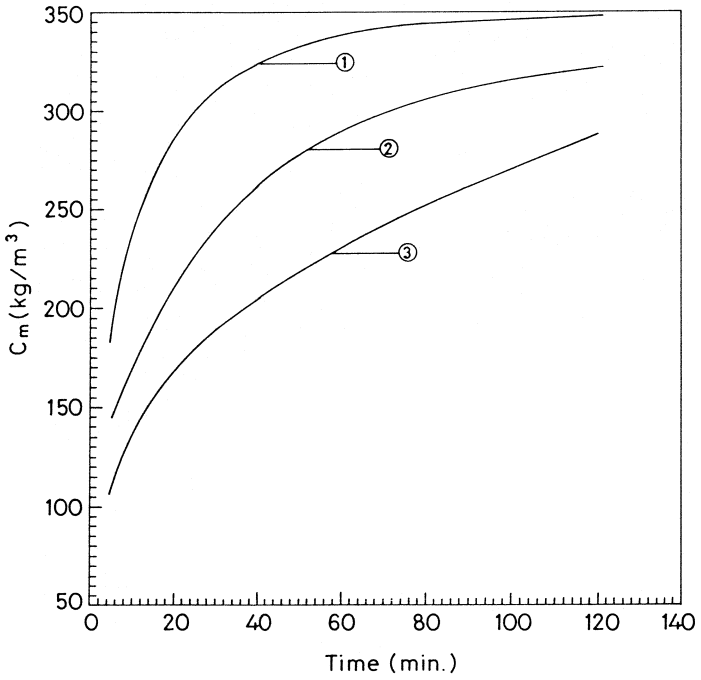

FIG. 3 Variation of membrane surface concentration (c_m) with time at different operating pressures and constant bulk concentration [results obtained at 25°C, with $R_m = 1.00014 \times 10^{14}$ m^{-1}, $\sigma = 0.9615$, and $c_b = 60$ kg/m^3. Simulated results: (1) 588.6 kPa, (2) 490.5 kPa, and (3) 392.4 kPa].

increases with the membrane surface concentration, the phenomenon of back-diffusion becomes more pronounced, and hence the rate of increase in the membrane surface concentration becomes small. The figure also suggests that the membrane surface concentration shows an increasing effect with pressure. As the pressure increases, the driving force for mass transfer is enhanced and the solute transportation rate to the surface increases. This implies that the rejection at the surface is higher and hence the membrane surface concentration is larger.

Figure 4 shows the variation of the relative permeate flux with time at different bulk concentrations when the applied pressure remains constant. The decreasing effect of flux with time can be accounted for because as time increases, more solute is rejected, giving rise to a higher negative osmotic pressure gradient over the membrane, resulting in a lowering of the effective driving force for transport across the membrane. The figure also shows a decreasing trend of flux with bulk concentration. As the bulk concentration increases, more solute is transported to the membrane surface, and a higher rejection rate results in a larger reverse osmotic pressure gradient and hence a lower effective driving force for mass transfer at a constant applied pressure differential.

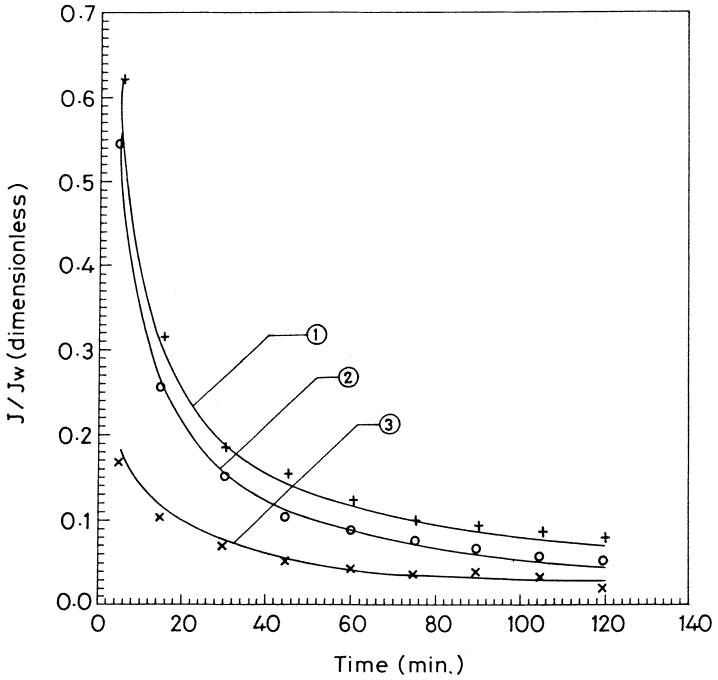

FIG. 4 Variation of relative permeate flux (J/J_w) with time at different bulk concentrations (c_b) and constant operating pressure [results obtained at 25°C, with $D = 1.50788 \times 10^{-10}$ m^2/s, $R_m = 1.00014 \times 10^{14}$ m^{-1}, $\sigma = 0.9615$, and $\Delta P = 490.5$ kPa. Simulated results: (1) 30 kg/m^3, (2) 45 kg/m^3, and (3) 60 kg/m^3. Experimental points: (+) 30 kg/m^3, (○) 45 kg/m^3, and (×) 60 kg/m^3].

The variation of the relative permeate flux as a function of time with different applied pressure differentials and a constant bulk concentration is shown in Fig. 5. The decline of flux with time is due to osmotic pressure, as stated earlier. As the pressure increases, the flux also increases due to a higher effective driving force. The increase is much more pronounced at lower time intervals but becomes sluggish as time increases. At a lower time value, a higher pressure differential directly increases the effective driving force, resulting in a higher flux. But this also causes the membrane surface concentration to increase substantially at a longer time, causing the rise in flux with pressure differential to be somewhat less than is to be expected. The simulated values are also shown in the figure, and they are in good agreement with the experimental results.

Permeate concentration as a function of time with different applied pressure differentials and constant bulk concentration is shown in Fig. 6(a). As ultrafiltration proceeds, the rejected solute is gradually accumulated near the membrane, causing a decline due to the effect of hindrance as stated earlier in the discussion of Fig. 1. An increase in pressure results in a higher permeate con-

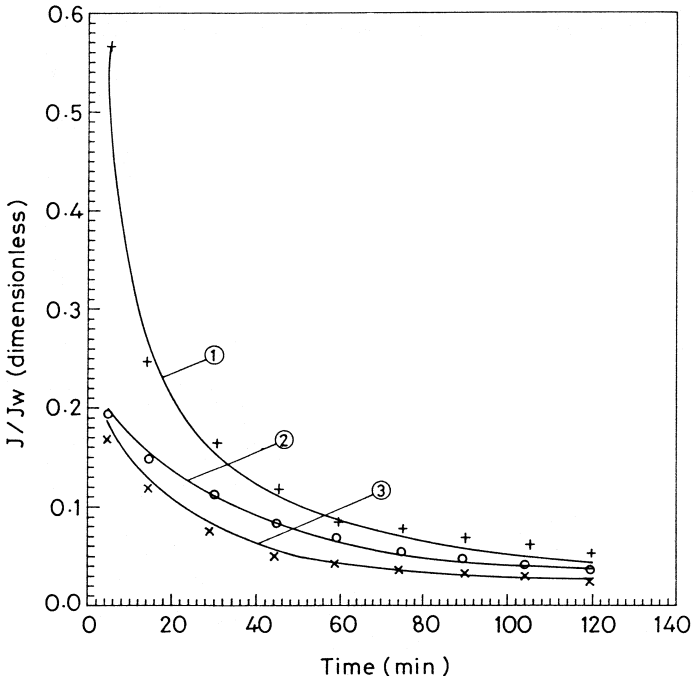

FIG. 5 Variation of relative permeate flux (J/J_w) with time at different operating pressures and constant bulk concentration [results obtained at 25°C, with $D = 1.50788 \times 10^{-10}$ m^2/s, $R_m = 1.00014 \times 10^{14}$ m^{-1}, $\sigma = 0.9615$, and $c_b = 45$ kg/m^3. Simulated results; (1) 588.6 kPa, (2) 490.5 kPa, and (3) 392.4 kPa. Experimental points: (+) 588.6 kPa, (○) 490.5 kPa, and (×) 392.4 kPa].

centration. Because it is a macromolecule, the entangled shape of PEG-6000 is oriented in the direction of the pore at high pressure and may pass through it. This gives a higher permeate concentration at a high pressure differential because more PEG molecules pass through the pores of the membrane. For nonmacromolecular solutes this effect may be opposite, thereby giving a smaller permeate concentration at higher pressure differentials because there is more compaction of the accumulated solute layer. Variation of solute rejection as a function of time for the same data set is shown in Fig. 6(b). Rejection increases with time mainly because the permeate concentration decreases as a function of time for the reason stated earlier. Also, the membrane surface concentration increases with time as shown in Fig. 3 for a different data set. The overall effect is an increase of rejection with time. A decrease in rejection with an increase in pressure is also evident from Fig. 6(b). As ΔP increases, c_p and c_m both increase, as shown earlier. A decrease of permeate concentration has been found to be dominant and so rejection increases with an increase in pressure. This increase is much more prominent at short times than it is after long times.

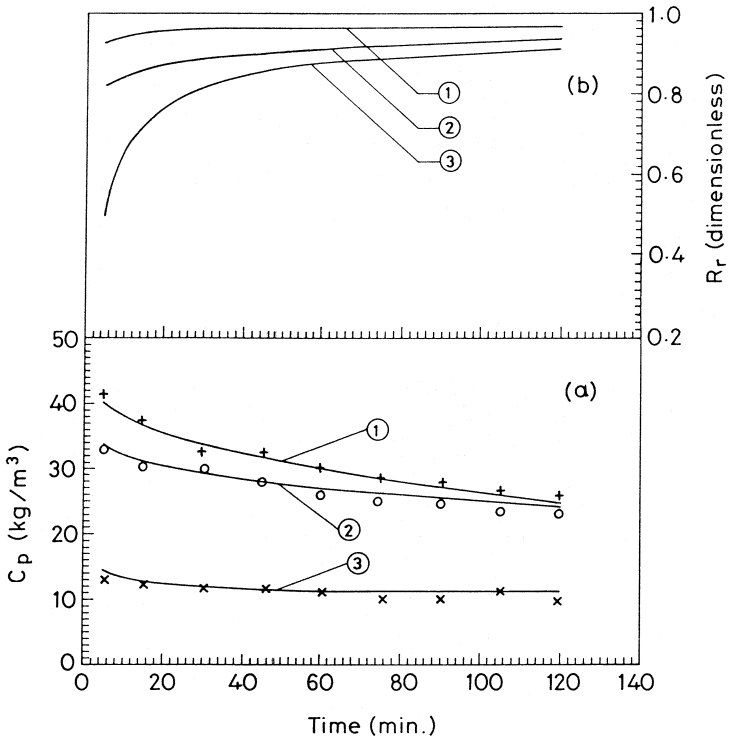

FIG. 6 (a) Plot of permeate concentration with time at different operating pressures and constant bulk concentration [results obtained at 25°C, with $D = 1.50788 \times 10^{-10}$ m^2/s, $R_m = 1.00014 \times 10^{14}$ m^{-1}, $\sigma = 0.9615$, and $c_b = 45$ kg/m^3. Simulated results: (1) 588.6 kPa, (2) 490.5 kPa, and (3) 392.4 kPa. Experimental points: (+) 588.6 kPa, (○) 490.5 kPa, and (×) 392.4 kPa]. (b) Plot of rejection with time at different operating pressures and constant bulk concentration [results obtained at 25°C, with $D = 1.50788 \times 10^{-10}$ m^2/s, $R_m = 1.00014 \times 10^{14}$ m^{-1}, $\sigma = 0.9615$, and $c_b = 45$ kg/m^3. Simulated results: (1) 588.6 kPa, (2) 490.5 kPa, and (3) 392.4 kPa].

CONCLUSION

A model based on an analytical solution of the governing boundary layer partial differential equation with pseudosteady-state assumptions has been attempted in this study. The concentration profile thus obtained has been coupled with an osmotic pressure model and irreversible thermodynamics to predict flux and rejection at any instant under specified operating conditions for ultrafiltration in an unstirred batch cell. The simulated results agree very well with the experimental data.

SYMBOLS

A', B'	constants used in Eq. (9)
B	dimensionless variable ($= Jz/2D$)

c	solute concentration (kg/m^3)
c_b	bulk solute concentration (kg/m^3)
c_m	solute concentration at membrane surface (kg/m^3)
c_p	solute concentration in the permeate (kg/m^3)
D	solute diffusivity (m^2/s)
F	parameter defined by Eq. (4)
J	volumetric permeate flux (m^3/m^2·s)
J_W	pure water flux (m^3/m^2·s)
M	molecular weight (kg/kmol)
MWCO	molecular weight cut off
P	hydraulic pressure (Pa)
P_m	solute permeability (m/s)
PEG	polyethylene glycol
Q	dimensionless variable ($= J/2)\sqrt{t/D}$
R	gas constant
R_r	"real" rejection, $1 - c_p/c_m$
S	dimensionless variable ($= z/2\sqrt{Dt}$)
R_m	membrane hydraulic resistance (m^{-1})
t	time (s)
T	absolute temperature in Eq. (2)
V_1, V_p	specific volume of solvent and polymer
x, x_1	parameters defined by Eq. (2)
z	distance from the membrane surface (m)

Greek Letters

γ_1, γ_2	parameters defined by Eq. (2)
μ	viscosity (Pa·s)
π	osmotic pressure (Pa)
ρ_p	density of polymer (kg/m^3)
σ	reflection coefficient (dimensionless)

REFERENCES

1. D. R. Trettin and M. R. Doshi, *Chem. Eng. Commun.*, *4*, 507 (1980).
2. J. S. Shen and R. F. Probstein, *Ind. Eng. Chem. Fundam.*, *16*, 459 (1977).
3. D. R. Trettin and M. R. Doshi, *Ibid.*, *19*, 189 (1980).
4. G. Belfort and N. Nagata, *Desalination*, *53*, 57 (1985).
5. P. Aimar and V. Sanchez, *Ind. Eng. Chem. Fundam.*, *25*, 789 (1986).
6. G. B. van den Berg and C. A. Smolders, *J. Membr. Sci.*, *73*, 103 (1992).
7. R. E. Lebrun, C. R. Bouchard, A. L. Rollin, T. Matsura, and S. Sourirajan, *Chem. Eng. Sci.*, *44*(2), 313 (1989).
8. L. Song and M. Elimelech, *J. Chem. Soc., Faraday Trans.*, *91*(19), 3389 (1995).
9. K. H. Youm, A. G. Fane, and D. E. Wiley, *J. Membr. Sci.*, *116*, 229 (1996).

MARCEL DEKKER, INC.
270 Madison Avenue, New York, New York 10016

10. C. Bhattacharjee and P. K. Bhattacharya, *J. Membr. Sci.*, *72*, 137 (1992).
11. C. Bhattacharjee and P. K. Bhattacharya, *Ibid*., *82*, 1 (1993).
12. S. Bhattacharjee and P. K. Bhattacharya, *Ibid*., *72*, 149 (1992).
13. S. De and P. K. Bhattacharya, *Ibid*., *109*, 109 (1996).
14. S. Redkar, V. Kuberkar, and R. H. Davis, *Ibid*., *121*, 229 (1996).
15. S. Bhattacharjee, A. Sharma, and P. K. Bhattacharya, *Ibid*., *111*, 243 (1996).
16. P. J. Flory, *Principles of Polymer Chemistry*, Cornell University Press, Ithaca, NY, 1953.
17. D. W. Van Krevelen and P. J. Hoftjer, *Properties of Polymers*, Elsevier, Amsterdam, 1977.
18. S. Nakao and S. Kimura, *J. Chem. Eng. Jpn*., *14*, 32 (1981).

Received by editor July 8, 1998
Revision received December 1998

Request Permission or Order Reprints Instantly!